



Fine balance of chemotactic and hydrodynamic torques: When microswimmers orbit a pillar just once

Chenyu Jin ¹, Jérémy Vachier,¹ Soumya Bandyopadhyay,² Tamara Macharashvili,³ and Corinna C. Maass ^{1,*}

¹Max Planck Institute for Dynamics and Self-Organization, Am Faßberg 17, 37077 Göttingen, Germany

²School of Mechanical Engineering, Purdue University, West Lafayette, Indiana 47907, USA

³Princeton University, Princeton, New Jersey 08544, USA



(Received 30 July 2019; published 24 October 2019)

We study the detention statistics of self-propelling droplet microswimmers attaching to microfluidic pillars. These droplets show negative autochemotaxis: they shed a persistent repulsive trail of spent fuel that biases them to detach from pillars in a specific size range after orbiting them just once. We have designed a microfluidic assay recording microswimmers in pillar arrays of varying diameter, derived detention statistics via digital image analysis, and interpreted these statistics via the Langevin dynamics of an active Brownian particle model. By comparing data from orbits with and without residual chemical field, we can independently estimate quantities such as hydrodynamic and chemorepulsive torques, chemical coupling constants and diffusion coefficients, as well as their dependence on environmental factors such as wall curvature. This type of analysis is generalizable to many kinds of microswimmers.

DOI: [10.1103/PhysRevE.100.040601](https://doi.org/10.1103/PhysRevE.100.040601)

Biological microswimmers operate in complex geometries and react to chemical and physical gradients, both external, e.g., in nutrients (chemotaxis [1–3]), and self-generated ones (autochemotaxis [4–6]), the latter enabling them to communicate and cooperate. The boundary conditions imposed, e.g., by soil packings and interfaces affect both the active dynamics of microswimmers, via hydrodynamic wall interactions [7,8] or active accumulation [9–11], as well as the diffusive spread of chemotactic fields. The coupling of these dynamics leads to complex feedback phenomena that can significantly influence behavior like arrest, aggregation, and biofilm formation [12].

In order to derive and test tractable models for systems featuring feedback it is important to develop experimental assays to decouple and control individual contributions. We have previously demonstrated one quite unexpected phenomenon in a highly tunable artificial model system, while studying the interaction of self-propelling droplet microswimmers with pillars in quasi-two-dimensional (quasi-2D) microfluidic cells (cf. [13–17]). These droplets shed a chemorepellent that biases them towards detachment after circling the pillar once [18]. Our system has the advantage of directly comparing wall attachment with and without chemotactic repulsion, as well as controllable curvature set by the pillar size.

In this Rapid Communication we present a quantitative study of the pillar interaction, analyzing the data from multiple experimental data sets in the context of an analytical

Langevin model for active Brownian particles (ABPs) incorporating hydrodynamic, chemotactic, and stochastic torques. This analysis provides insight into the respective strengths of wall attraction, chemorepulsion, as well as rotational diffusion and their effects on interfacial capture. As is it based on ABP models, it can be generalized to many microswimmers.

Our microswimmers consist of oil droplets dissolving gradually in a micellar aqueous surfactant solution, on a timescale of up to several hours. The oil solubilizes by diffusing into surfactant micelles in a boundary layer around the droplet, a process that also depletes the surfactant coverage of the droplet's oil-water interface [19,20]. If the droplet position fluctuates, filled micelles trail behind it, such that there are more empty micelles at its anterior. Empty micelles can disintegrate to replenish the surfactant coverage at the interface: thus, a moving droplet has more surfactant at its anterior, leading to a self-sustaining gradient in interfacial tension towards the posterior and a force propelling the droplet ($v \approx 30\text{--}60 \mu\text{m s}^{-1}$). Chemotaxis and autochemotaxis follow naturally from the droplets' mechanism of propulsion [21]. Droplets are attracted by empty micelles, such that they follow surfactant gradients (chemotaxis) and avoid areas of filled micelles, which act as a chemorepellent. The micelles diffuse slowly in comparison to the droplet motion, with a diffusion constant $D_m \approx 100 \mu\text{m}^2 \text{s}^{-1}$ [22], such that the repulsive trail of filled micelles persists over long times. We have experimentally confirmed [21] that this negative autochemotaxis is mediated by the diffusion of filled micelles.

To render a statistical analysis of the pillar interactions possible, we required experimental data on a large number of events, using monodisperse oil droplets and pillars from a range of radii. The oil phase consisted of a mixture of the nematogen 4-pentyl-4'-cyano-biphenyl (5CB) and 1-bromopentadecane at a volume ratio of 10:1. We chose droplets of this isotropic mixture, as they perform a persistent

*corinna.maass@ds.mpg.de

Published by the American Physical Society under the terms of the [Creative Commons Attribution 4.0 International](https://creativecommons.org/licenses/by/4.0/) license. Further distribution of this work must maintain attribution to the author(s) and the published article's title, journal citation, and DOI.

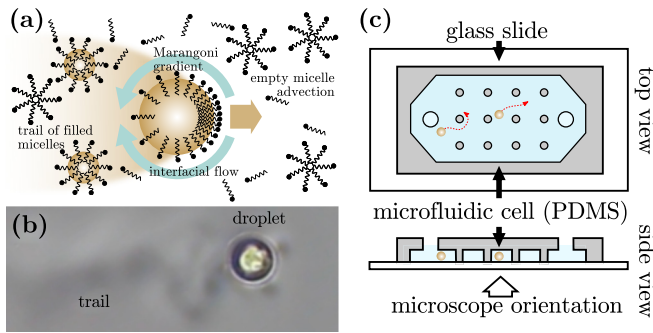


FIG. 1. (a) Schematic of the droplet propulsion via interfacial Marangoni gradients. (b) Phase contrast image of a swimming droplet, dragging a trail of filled micelles visible due to refractive index variation. Figure adapted from [21]. (c) Schematic of droplets in a quasi-2D PDMS cell containing a pillar array.

Brownian motion, while droplets of pure 5CB exhibit a strong curling instability [23]. We mass-produced monodisperse droplets in flow-focusing microfluidic devices [24].

We fabricated quasi-2D polydimethylsiloxane (PDMS) reservoirs bonded to glass slides using standard soft lithography protocols [25]. The reservoirs were approximately $6 \text{ mm} \times 10 \text{ mm} \times 116 \mu\text{m}$ in size and contained arrays of 18 or 32 micropillars with radii chosen from $r \in \{50, 75, 100, 250\} \mu\text{m}$ [Fig. 1(c)]. Data sets for even larger pillar sizes are included in the Supplemental Material (SM) [26] and Refs. [27–38] therein. We have not included these data in our detachment analysis, since the droplets are effectively trapped at these pillars.

We filled the reservoirs with a swimming medium, specifically an aqueous solution of the ionic surfactant tetracycltrimethylammonium bromide at 7.5 wt%, containing between 5 and 20 droplets of radius $a \approx 50 \mu\text{m}$ per sample. We recorded the droplet motion via bright field video microscopy, typically over 5 to 10 minutes with up to 200 pillar interactions per run. Each experiment was repeated multiple times, yielding between 1000 and 2500 interactions per pillar size in total. We extracted individual trajectories by numerical image analysis, using a Crocker-Grier algorithm [27,28]. Pillar locations and sizes were calibrated via the respective lithography template. Speed, angular velocity, distance, and orientation with respect to each pillar were extracted from the recorded coordinates. We preselected attached trajectory segments via a distance criterion and refined them by an attachment angle threshold. By restricting the analysis to “clean” pillars without residual chemorepellent from previous interactions, we retained between 350 and 800 interactions per pillar size. We provide detailed statistics and experimental protocols in the SM [26].

Autochemotactic droplets interacting with pillars in a quasi-2D cell show specific dynamics: A persistent microswimmer will not successfully attach to a convex wall without an attractive torque. Since the required torque increases with curvature, microswimmers experiencing a finite wall attraction are expected to scatter off small pillars and get trapped at large ones [13–15]. Our droplets are attracted to walls and indeed exhibit scattering from small pillars and trapping at large pillars. However, at pillars of intermediate

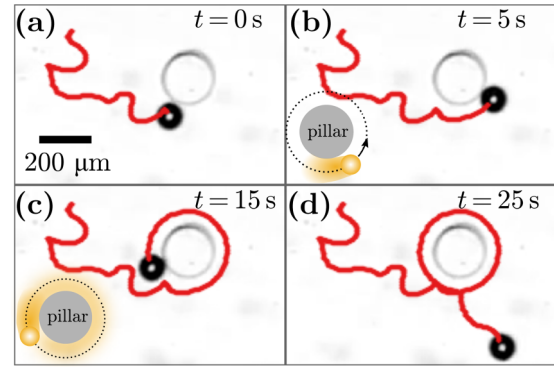


FIG. 2. A negatively autochemotactic droplet ($a = 50 \mu\text{m}$) interacting with a pillar ($R = 100 \mu\text{m}$). (a) The droplet attaches to the pillar, (b), (c) travels around the pillar, and (d) detaches soon after it reenters its own trail (red line: trajectory).

radii, we observe a significant increase of detachment after circling the pillar once, i.e., when droplets approach and reenter their own trajectory [18]: the filled micelles diffuse away from the pillar [Fig. 4(c)], providing an additional chemorepulsive gradient and favoring detachment. We illustrate this by consecutive video stills of a typical interaction with a $100 \mu\text{m}$ pillar in Fig. 2 and a histogram of detention lengths for many similar interactions in Fig. 3, which clearly shows a peak around lengths corresponding to one orbit (see also the movie in the SM [26]).

The long-tailed peaks in the statistics of detention times suggest stochastic influences on the pillar interaction [29,39]. Rotational noise and convex curvature cause a fraction of droplets to detach almost immediately (Fig. 3, blue peak). For droplets attached long enough to approach their own residual chemical field, we can distinguish two cases: If the chemical repulsion is too strong to allow the droplets to reenter their trajectory, this creates a *noncrossing* peak in the histogram of detention lengths slightly before one full orbit (green). Otherwise, the droplet is forced to swim along its own trail, as traced in Fig. 2. However, the added chemotactic repulsion adds a bias towards detachment, resulting in a *self-crossing* peak in the histogram of detention lengths slightly after one orbit (yellow). We exclude data from noncrossing interactions from our analysis, since their chemical interactions break radial symmetry and would require rather sophisticated modeling.

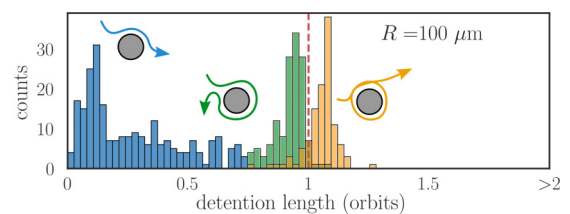


FIG. 3. Example histogram of the detention lengths of droplets ($a = 50 \mu\text{m}$) at a pillar ($R = 100 \mu\text{m}$). Color codes and sketches illustrate the cases of scattering (blue), noncrossing (green), and self-crossing (orange) trajectories. We bin by length for illustration purposes; in the remainder of the study data is binned by time to match the theory model.

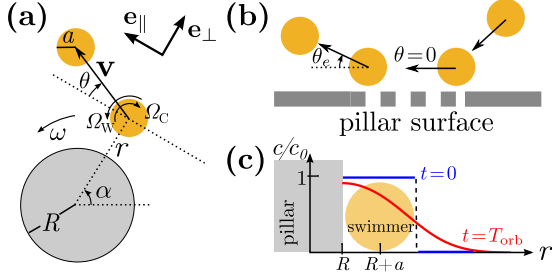


FIG. 4. Model schematics and coordinate definitions. (a) A droplet of radius a moving around a pillar of radius R with velocity \mathbf{v} and angular velocity ω , torques from chemotactic, Ω_C , and wall interaction, Ω_W , and polar coordinates (r, α) . (b) Schematic drawing of a droplet approaching and leaving a pillar, with escape angle θ_e . (c) Chemorepellent diffusion away from the pillar [numerical solution of Eq. (5) for $R = a$]. Radial concentration c/c_0 vs r , with the initial step function (dotted, blue) for $t = 0$ and the diffused profile (solid, red) for $t = T_{\text{orb}}$.

We can already estimate the forces and torques of interest from the following simple analytical model applied to the cases of short-time scattering and self-crossing.

For a quantitative estimate of the effects of curvature, wall interaction, and autochemotaxis we model our droplets as ABPs [40–42]. The ABP paradigm is widely used to model both artificial [30] and biological [43] microswimmers subject to fluctuations. In this context, self-propulsion is seen as an effective driving force which can be easily added to other forces in the system [44].

The droplet is represented by a point particle moving with speed v ; its position \mathbf{r} and direction \mathbf{e} are described by the overdamped Langevin equations

$$\dot{\mathbf{r}} = v\mathbf{e}, \quad \dot{\mathbf{e}} = (\boldsymbol{\Omega} + \sqrt{2D_R}\boldsymbol{\xi}) \times \mathbf{e}. \quad (1)$$

$\boldsymbol{\Omega}$ is the sum of deterministic drifts of \mathbf{e} ; the rotational fluctuations are modeled by the rotational diffusivity D_R and a normalized zero-mean Gaussian white noise $\boldsymbol{\xi}$ with variance $\langle \xi_i(t)\xi_j(t') \rangle = \delta_{ij}\delta(t-t')$. We note that the orientation of self-propelling droplets can be affected by both whole body rotations and shifts in interfacial tension. However, in our reduction to point particles, these revert to effective forces and torques.

The droplet motion is restricted to the xy plane, with a perpendicular $\boldsymbol{\Omega} = (0, 0, \Omega)^T$. In our system $\Omega = \Omega_W + \Omega_C$ comprises the external (mostly hydrodynamic) torque due to wall attraction, Ω_W , and autochemotaxis, Ω_C , from the second orbit. A schematic representation of the system is shown in Fig. 4(a). We use polar coordinates (r, α) with the origin $r = 0$ at the center of a pillar of radius R , with a droplet of radius a at the position \mathbf{r} . We project the orientational unit vector of the droplet \mathbf{e} on two orthogonal unit vectors, \mathbf{e}_\perp perpendicular and \mathbf{e}_\parallel tangential to the pillar interface. We define $\theta \in [-\pi/2, \pi/2]$ as the angle between \mathbf{e} and \mathbf{e}_\parallel , with $\theta \approx 0$ when the droplet is moving along the pillar tangent. Without loss of generality, we assume the droplet to move counterclockwise around the pillar, such that it approaches with $\theta > 0$ and detaches with $\theta < 0$. From Eq. (1), we

derive [29]

$$\dot{r} = \dot{\mathbf{r}} \cdot \mathbf{e}_\perp = -v \sin \theta, \\ \dot{\theta} = -\omega + \Omega + \sqrt{2D_R}\xi, \quad \text{with } \omega = \frac{1}{r}(\dot{\mathbf{r}} \cdot \mathbf{e}_\parallel), \quad (2)$$

where $\omega > 0$ is the angular velocity of the droplet around the pillar. The droplet detaches when θ exceeds a fixed escape angle θ_e [29,39] [Fig. 4(b)]. The detention time t_d is therefore the first-passage time of θ_e of a stochastic process described by Eq. (2). Here we take $\theta_0 = 0$, and $\theta_e = -0.962$ as the escape angle measured at the moment of detachment (see SM [26]).

Our restriction to counterclockwise motion would in principle necessitate a reflective boundary condition for $\theta_r = \pi/2$; however, for moderate rotational diffusion D_R (see SM [26]), this head-on orientation is hydrodynamically unlikely in the case of our highly persistent pusher-type droplets [19,23] even in the limiting case of zero wall curvature and no chemotactic wall repulsion, and the boundary condition can be safely neglected.

Generally, Ω_W and Ω_C are functions of $r(t)$, $\theta(t)$, and $\alpha(t)$, depending on the exact nature of the hydrodynamic and chemical fields. However, we can treat them as constants using the following approximations. We assume the transition between an attached and a detached state to be instantaneous compared to the detention time, such that $r \approx R + a$, $\theta \approx 0$ and Ω_W is constant for the droplet while it is attached. We note that we cannot expect Ω_W to be the same for all pillar sizes, if the length scales of pillar, droplet, and flow field, e.g., puller dipole size, are comparable (cf. [7]).

The recorded angular speeds ω are quite uniform in each orbit (see SM [26]), with a slight slowdown in the second orbit, when the droplet moves on its own trail. We therefore treat ω as constant within one orbit, with $\omega \in \omega_1, \omega_2$.

For $(\omega_1 - \omega_2)/\omega_1 \ll 1$ [cf. Fig. 6(b)], we can further assume that the orbiting period T_{orb} of the droplet does not significantly increase with time, such that the droplet always experiences the same chemical gradient $\partial_r c(t)|_{r=R+a}$ initiated during its previous passage. We therefore approximate Ω_C as constant between the points where the droplet has fully crossed over onto its trail and where it leaves the pillar, and we define the detention time $t_d - T_{\text{orb}}$ in the second orbit as the time elapsed between these two events.

Under these approximations of constant Ω_W , Ω_C , and ω , the detention time t_d follows an inverse Gaussian distribution

$$f(t_d; \mu, \lambda) = \sqrt{\frac{\lambda}{2\pi t_d^3}} \exp\left[-\frac{\lambda(t_d - \mu)^2}{2\mu^2 t_d}\right], \quad (3)$$

with $\lambda = \theta_e^2/2D_R$ and the distribution mean $\mu = \langle t_d \rangle = \theta_e/(\Omega - \omega)$.

If the deterministic torque compensates the geometry effect, the drift $\Omega - \omega$ is zero, and μ diverges. In this case, $f(t_d)$ reverts to a Lévy distribution

$$f(t_d) = \sqrt{\frac{\lambda}{2\pi t_d^3}} \exp\left[\frac{-\lambda}{2t_d}\right]. \quad (4)$$

We have tested our approximations for the case of a straight wall without drift by calculating $f(t_d)$ using a less

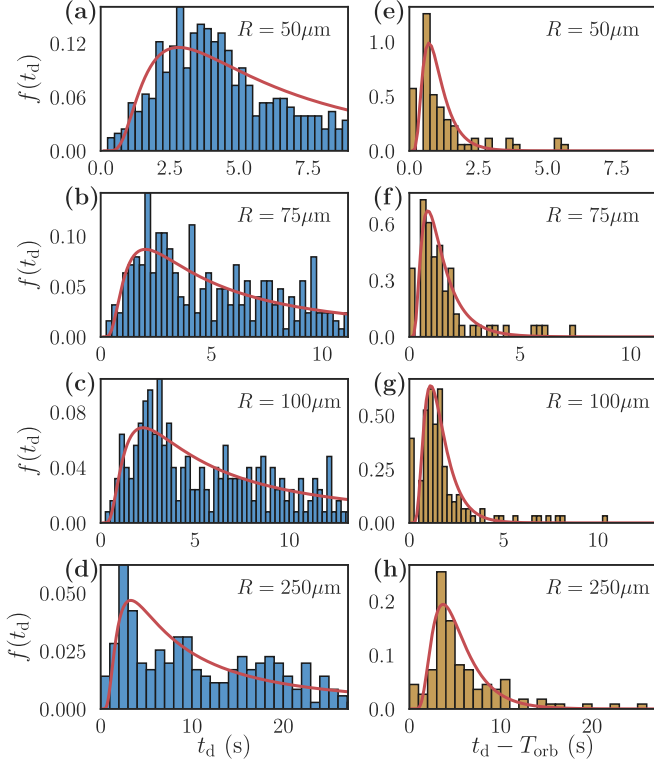


FIG. 5. Normalized histograms $f(t_d)$ of the detention times of $a = 50 \mu\text{m}$ droplets at pillars of varying radii R , first [blue, panels (a)–(d)] and second, self-crossing [yellow, panels (e)–(h)] orbits. The t origin of the latter is reset to T_{orb} for each trajectory. Red lines: inverse Gaussian fits, first orbit fitted only for $t < 0.7T_{\text{orb}}$ to rule out noncrossing chemotactic detachments.

approximative Fokker-Planck model [38,39] that includes the reflective boundary condition. The difference to the corresponding Lévy distribution is indeed too small to be resolved in experimental statistics (see [26]).

We numerically approximate the concentration field $c(r, \alpha)$ of filled micelles in the polar coordinate system (r, α) (Fig. 4). We assume that a droplet of radius a dissolves at a constant rate and approximate its initial trail of filled micelles by a step function, $c(R < r < R + 2a) = c_0$, which we let diffuse over time, using the micellar diffusion coefficient $D_m \approx 100 \mu\text{m}^2 \text{s}^{-1}$.

Under the boundary conditions $\partial_r c|_{r=R} = 0$ and $c(r \rightarrow +\infty) = 0$ we solve the diffusion equation

$$\partial_t c = D_m \partial_r (r \partial_r c) / r, \quad (5)$$

numerically using a forward-marched explicit finite difference scheme. For illustration, we plot in Fig. 4(c) the rescaled filled micelle concentrations c/c_0 behind a droplet attached to a pillar with $R = a$, diffusing from a step function at $t = 0$ (dashed, blue) to a smoothed profile (solid, red) at $t = T_{\text{orb}}$. Calculated profiles and derivatives for our experimental settings are listed in the SM [26].

We have sorted all attachment events into scattering, self-crossing, and noncrossing events (Fig. 3; see the SM [26] for image analysis criteria and statistical quantities) and extracted the quantities t_d , $v(t)$, $\omega(t)$, and $\theta(t)$. Figure 5 contains two subsets of detention time distributions for increasing pillar sizes and the respective inverse Gaussian fits of Eq. (3). The first set (blue) contains the data range for $0 < t_d < 0.7T_{\text{orb}}$ with $\Omega_C = 0$. The second set (yellow, only self-crossing) is taken from the moment T_{orb} where the droplet crosses its own trajectory and $\Omega_C = \text{const}$.

Using the extracted fitting parameters μ, λ from Eq. (3) and the measured ω , we calculate D_R , Ω_W , and Ω_C for each pillar size, as well as the expectation value of the detention times $\langle t_d \rangle = \mu$, as plotted in Fig. 6. As expected, $\langle t_d \rangle$ is larger in the first orbit [Fig. 6(a)], where $\Omega_C = 0$, and increases with increasing R , in fact diverging for $\Omega_C = 0$ and $R \in \{100, 250\} \mu\text{m}$, indicating a trapped state in the absence of Ω_C . We note that this transition to the trapped state would not stand out in an analysis based on averaged recorded detention times [13,15], since these are bounded by the duration of the experiment and therefore cannot diverge.

The recorded mean orbital speeds $\langle |\omega| \rangle$ scale linearly with $(R + a)^{-1}$ and do not change significantly between orbits 1 and 2, justifying our approximation of an overall constant speed [Fig. 6(b)].

The extracted torques [Fig. 6(c)] permit a number of observations: both Ω_W and $-\Omega_C$ decrease with pillar size, the latter simply because orbiting takes longer and the chemorepulsive gradient $\partial_r c$ decreases by diffusion, the former possibly because the pusher-type hydrodynamic interactions depend on wall curvature [7]. Ω_C overcompensates Ω_W in all cases up to $R = 250 \mu\text{m}$, explaining the enhanced detachment after one

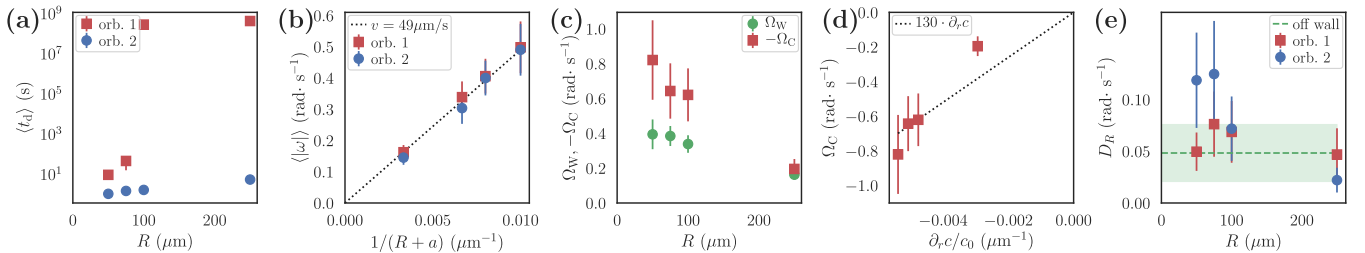


FIG. 6. Extracted parameters for detention statistics of $a = 50 \mu\text{m}$ at pillars with $R \in \{50, 75, 100, 250\} \mu\text{m}$, values for first and second orbits. (a) Measured detention times. (b) Measured orbital speed vs curvature. (c) Wall attraction Ω_W and negative chemorepulsion $-\Omega_C$ torques, from fits. (d) Ω_C vs calculated chemical gradient. (e) Rotational diffusion coefficient, from fits, green dashed line and shaded confidence interval: free motion between pillars. Numerical values and error discussion in the SM [26].

orbit and the transition to fully trapped states for $R > 250 \mu\text{m}$. Similarly, the diverging detention times in the first orbit for $R \in \{100, 250\} \mu\text{m}$ are due to the fact that Ω_{W} compensates ω while $\Omega_{\text{C}} = 0$.

For an estimate of the chemotactic coupling, we have plotted the fitted Ω_{C} versus the calculated filled micelle gradient, $\partial_r c(t)/c_0$, using Eq. (5) [Fig. 6(d)]. If we assume a linear dependence on the filled micelle gradient [21,45], $\Omega_{\text{C}} = \kappa \partial_r c/c_0$, linear regression yields $\kappa \approx 130 \text{ rad } \mu\text{m s}^{-1}$ with c_0 on the order of 200 oil molecules per μm^3 (see SM [26]). However, this should be regarded as no more than an order-of-magnitude estimate due to our limited range of accessible pillar sizes ($50 \mu\text{m} < R < 250 \mu\text{m}$) and the various approximations in our model.

In Fig. 6(e), we plot the extracted rotational diffusion coefficients, D_{R} . For comparison, we have estimated an average $D_{\text{R}} \approx 0.05 \text{ rad s}^{-1}$ of droplets moving freely between pillars based on their rotational persistence (see SM [26]). The values for droplets at pillars are comparable to the freely swimming case. We note a slight elevation at small pillars in the presence of chemotactic gradients; however, since our approximations grow less accurate with decreasing pillar size, this deviation can be expected.

The fact that the rotational diffusion estimates for freely moving and wall attached droplets are comparable is not intuitively obvious, since variations in interfacial tension provide a major source of noise and such variations are affected by the boundary conditions of advective flow and chemical fields. Our data suggests that the differences are small enough to treat

the rotational diffusion coefficient of a droplet microswimmer as a meaningful physical quantity.

We have shown that from a simple curious phenomenon—droplets leaving pillars after orbiting them just once—one can independently estimate various quantities such as hydrodynamic and chemorepulsive torques, diffusion coefficients, and their dependence on wall curvature by a statistical analysis of detention times and their interpretation using an ABP model. This provides valuable insight into droplet microswimmers in particular, where many of these quantities are hard to access independently or where their sensitivity to boundary conditions is still open to debate.

Moreover, since the ABP model makes no assumptions about the details of the propulsion process, this assay and analysis can also be extended to probe similar quantities in various other microswimmer systems.

It can also be used to include other external forces represented by additional drift terms, for example, the effects of gravity on detention time and wall accumulation [46] or steric phenomena for nonspherical microswimmers influencing the reorientation dynamics at the wall [47]. In consequence, the model presented here offers a systematic approach to studying the behavior of artificial as well as biological microswimmers close to a boundary.

We acknowledge Babak V. Hokmabad for experimental, and Fabian Schwarzendahl and Babak Nasouri for theoretical advice. This project was partially funded by the MPI-DS Prandtl internship program and the MaxSynBio consortium.

-
- [1] M. T. Madigan and J. M. Martinko, *Bacterial cell surface structures*, in *Brock Biology of Microorganisms* (Pearson Education, Limited, 2005), Chap. 4.
 - [2] J. Adler, Chemotaxis in bacteria, *Science* **153**, 708 (1966).
 - [3] G. L. Hazelbauer, Bacterial chemotaxis: The early years of molecular studies, *Annu. Rev. Microbiol.* **66**, 285 (2012).
 - [4] J. T. Bonner and L. J. Savage, Evidence for the formation of cell aggregates by chemotaxis in the development of the slime mold *Dictyostelium discoideum*, *J. Exp. Zool.* **106**, 1 (1947).
 - [5] K. Zhao, B. S. Tseng, B. Beckerman, F. Jin, M. L. Gibiansky, J. J. Harrison, E. Luijten, M. R. Parsek, and G. C. L. Wong, Psl trails guide exploration and microcolony formation in *Pseudomonas aeruginosa* biofilms, *Nature (London)* **497**, 388 (2013).
 - [6] C. R. Reid, T. Latty, A. Dussutour, and M. Beekman, Slime mold uses an externalized spatial “memory” to navigate in complex environments, *Proc. Natl. Acad. Sci. U.S.A.* **109**, 17490 (2012).
 - [7] S. E. Spagnolie and E. Lauga, Hydrodynamics of self-propulsion near a boundary: Predictions and accuracy of far-field approximations, *J. Fluid Mech.* **700**, 105 (2012).
 - [8] A. P. Berke, L. Turner, H. C. Berg, and E. Lauga, Hydrodynamic Attraction of Swimming Microorganisms by Surfaces, *Phys. Rev. Lett.* **101**, 038102 (2008).
 - [9] G. Li and J. X. Tang, Accumulation of Microswimmers near a Surface Mediated by Collision and Rotational Brownian Motion, *Phys. Rev. Lett.* **103**, 078101 (2009).
 - [10] S. van Teeffelen and H. Löwen, Dynamics of a Brownian circle swimmer, *Phys. Rev. E* **78**, 020101(R) (2008).
 - [11] J. Elgeti and G. Gompper, Wall accumulation of self-propelled spheres, *Europhys. Lett.* **101**, 48003 (2013).
 - [12] I. Tuval, L. Cisneros, C. Dombrowski, C. W. Wolgemuth, J. O. Kessler, and R. E. Goldstein, Bacterial swimming and oxygen transport near contact lines, *Proc. Natl. Acad. Sci. U.S.A.* **102**, 2277 (2005).
 - [13] O. Sipoș, K. Nagy, R. Di Leonardo, and P. Galajda, Hydrodynamic Trapping of Swimming Bacteria by Convex Walls, *Phys. Rev. Lett.* **114**, 258104 (2015).
 - [14] D. Takagi, J. Palacci, A. B. Braunschweig, M. J. Shelley, and J. Zhang, Hydrodynamic capture of microswimmers into sphere-bound orbits, *Soft Matter* **10**, 1784 (2014).
 - [15] J. Simmchen, J. Katuri, W. E. Uspal, M. N. Popescu, M. Tasinkevych, and S. Sánchez, Topographical pathways guide chemical microswimmers, *Nat. Commun.* **7**, 10598 (2016).
 - [16] M. Contino, E. Lushi, I. Tuval, V. Kantsler, and M. Polin, Microalgae Scatter Off Solid Surfaces by Hydrodynamic and Contact Forces, *Phys. Rev. Lett.* **115**, 258102 (2015).
 - [17] M. Brun-Cosme-Bruny, E. Bertin, B. Coasne, P. Peyla, and S. Rafai, Effective diffusivity of microswimmers in a crowded environment, *J. Chem. Phys.* **150**, 104901 (2019).
 - [18] C. Jin, B. Vajdi Hokmabad, K. A. Baldwin, and C. C. Maass, Chemotactic droplet swimmers in complex geometries, *J. Phys.: Condens. Matter* **30**, 054003 (2018).

- [19] S. Herminghaus, C. C. Maass, C. Krüger, S. Thutupalli, L. Goehring, and C. Bahr, Interfacial mechanisms in active emulsions, *Soft Matter* **10**, 7008 (2014).
- [20] C. C. Maass, C. Krüger, S. Herminghaus, and C. Bahr, Swimming droplets, *Annu. Rev. Condens. Matter Phys.* **7**, 171 (2016).
- [21] C. Jin, C. Krüger, and C. C. Maass, Chemotaxis and autochemotaxis of self-propelling droplet swimmers, *Proc. Natl. Acad. Sci. U.S.A.* **114**, 5089 (2017).
- [22] S. Candau, E. Hirsch, and R. Zana, New aspects of the behaviour of alkyltrimethylammonium bromide micelles: Light scattering and viscosimetric studies, *J. Phys.* **45**, 1263 (1984).
- [23] C. Krüger, G. Klös, C. Bahr, and C. C. Maass, Curling Liquid Crystal Microswimmers: A Cascade of Spontaneous Symmetry Breaking, *Phys. Rev. Lett.* **117**, 048003 (2016).
- [24] T. Thorsen, R. W. Roberts, F. H. Arnold, and S. R. Quake, Dynamic Pattern Formation in a Vesicle-Generating Microfluidic Device, *Phys. Rev. Lett.* **86**, 4163 (2001).
- [25] D. Qin, Y. Xia, and G. M. Whitesides, Soft lithography for micro- and nanoscale patterning, *Nat. Protoc.* **5**, 491 (2010).
- [26] See Supplemental Material at <http://link.aps.org/supplemental/10.1103/PhysRevE.100.040601> for experimental protocols, data tables, and theory appendix.
- [27] J. C. Crocker and D. G. Grier, Methods of digital video microscopy for colloidal studies, *J. Colloid Interface Sci.* **179**, 298 (1996).
- [28] C. Krüger, Liquid crystal microswimmers—From single entities to collective dynamics, Ph.D. thesis, University of Göttingen, 2016.
- [29] S. E. Spagnolie, G. R. Moreno-Flores, D. Bartolo, and E. Lauga, Geometric capture and escape of a microswimmer colliding with an obstacle, *Soft Matter* **11**, 3396 (2015).
- [30] J. R. Howse, R. A. L. Jones, A. J. Ryan, T. Gough, R. Vafabakhsh, and R. Golestanian, Self-Motile Colloidal Particles: From Directed Propulsion to Random Walk, *Phys. Rev. Lett.* **99**, 048102 (2007).
- [31] J. Saragosti, P. Silberzan, and A. Buguin, Modeling *E. coli* tumbles by rotational diffusion. Implications for chemotaxis, *PLoS One* **7**, e35412 (2012).
- [32] K. Drescher, J. Dunkel, L. H. Cisneros, S. Ganguly, and R. E. Goldstein, Fluid dynamics and noise in bacterial cell–cell and cell–surface scattering, *Proc. Natl. Acad. Sci. U.S.A.* **108**, 10940 (2011).
- [33] R. Grundmann, Boundary layer equations and methods of solution, in *Computational Fluid Dynamics*, edited by J. F. Wendt (Springer, Berlin, Heidelberg, 2009), pp. 153–181.
- [34] V. V. Konotop and L. Vazquez, *Nonlinear Random Waves* (World Scientific, Singapore, 1994).
- [35] T. D. Frank, Delay Fokker-Planck equations, perturbation theory, and data analysis for nonlinear stochastic systems with time delays, *Phys. Rev. E* **71**, 031106 (2005).
- [36] E. A. Novikov, Functionals and the random-force method in turbulence theory, *Zh. Eksp. Teor. Fiz.* **47**, 1919 (1965) [*Sov. Phys. JETP* **20**, 1290 (1965)].
- [37] J. Zinn-Justin, *Quantum Field Theory and Critical Phenomena* (Oxford University Press, New York, 2002).
- [38] J. Vachier and M. G. Mazza, Dynamics of sedimenting active Brownian particles, *Eur. Phys. J. E* **42**, 11 (2019).
- [39] K. Schaar, A. Zöttl, and H. Stark, Detention Times of Microswimmers Close to Surfaces: Influence of Hydrodynamic Interactions and Noise, *Phys. Rev. Lett.* **115**, 038101 (2015).
- [40] M. Schmitt and H. Stark, Active Brownian motion of emulsion droplets: Coarsening dynamics at the interface and rotational diffusion, *Eur. Phys. J. E* **39**, 80 (2016).
- [41] P. Romanczuk, M. Bär, W. Ebeling, B. Lindner, and L. Schimansky-Geier, Active Brownian particles: From individual to collective stochastic dynamics, *Eur. Phys. J.: Spec. Top.* **202**, 1 (2012).
- [42] C. Bechinger, R. Di Leonardo, H. Löwen, C. Reichhardt, G. Volpe, and G. Volpe, Active particles in complex and crowded environments, *Rev. Mod. Phys.* **88**, 045006 (2016).
- [43] I. Rushkin, V. Kantsler, and R. E. Goldstein, Fluid Velocity Fluctuations in a Suspension of Swimming Protists, *Phys. Rev. Lett.* **105**, 188101 (2010).
- [44] A. Zöttl and H. Stark, Emergent behavior in active colloids, *J. Phys.: Condens. Matter* **28**, 253001 (2016).
- [45] J. Taktikos, V. Zaburdaev, and H. Stark, Modeling a self-propelled autochemotactic walker, *Phys. Rev. E* **84**, 041924 (2011).
- [46] J. Palacci, C. Cottin-Bizonne, C. Ybert, and L. Bocquet, Sedimentation and Effective Temperature of Active Colloidal Suspensions, *Phys. Rev. Lett.* **105**, 088304 (2010).
- [47] A. Wysocki, J. Elgeti, and G. Gompper, Giant adsorption of microswimmers: Duality of shape asymmetry and wall curvature, *Phys. Rev. E* **91**, 050302(R) (2015).